Experimental and Theoretical Study of the Br···N Halogen Bond in Complexes of 1,4-Dibromotetrafluorobenzene with Dipyridyl Derivatives

Alessandra Forni[†]

CNR-ISTM, Institute of Molecular Sciences and Technologies, via Golgi 19, 20133 Milano, Italy

Received: December 5, 2008; Revised Manuscript Received: January 30, 2009

The electron density distributions of two halogen-bonded complexes, that is, (*E*)-1,2-bis(4-pyridyl)ethylene (bpe) or 4,4′-dipyridyl (dp) with 1,4-dibromotetrafluorobenzene ($C_6F_4Br_2$), have been obtained from accurate single-crystal X-ray diffracted intensities collected at 90 K and analyzed through the Bader's quantum theory of atoms in molecules. The experimental results have been compared with theoretical densities resulting from DFT calculations on both gas-phase isolated complexes and periodic crystal structures. The topological features and the energetics of the underlying Br···N intermolecular halogen bonding connecting bpe and dp with $C_6F_4Br_2$ molecules into 1D infinite chains have been investigated and compared with the previously analyzed I···N halogen bond. The analysis provides a quantitative evaluation of the differences observed between the involved halogen species, in addition to pointing out the basic features shared by the investigated halogen bond interactions.

1. Introduction

Halogen bonding,[1] namely, any noncovalent interaction involving halogens as electrophilic species, has been long ago recognized to play a crucial role in fields as disparate as crystal engineering,[2] material science,[3] and molecular biology.[4] For example, the importance of halogen bonding in recognition processes involving thyroid hormones, a class of tyrosine-based hormones containing iodine, is documented by the exceptionally short I···O contact observed in the complex of thyroxine (3,5,3′,5′-tetraiodo-L-thyronine) with its transport protein transthyretin (distance, 3.07 Å).[5] A short Br···O contact has been as well observed in an aldose reductase complex with a brominated inhibitor (distance, 3.0 Å).[6]

The great potential of halogen bonding in the design of new and high-value functional materials, ranging from organic semiconductors[3a,b] to liquid crystals,[3c,d] electrooptical devices,[3e−g] and magnetic materials,[3h] is now widely recognized.

The first studies on the use of halogen bonding for crystal engineering purposes date back to the middle of the 20th century, when the structural aspects of 1:1 complexes of halogen molecules or simple halocarbons, such as diiodoacethylene or tetrabromoethylene, with molecules containing O, N, S, or Se have been investigated.[7] More recently, haloperfluoroalkanes and -arenes have been demonstrated to be very robust tectons thanks to the strength and directionality of the halogen bond they form, allowing an optimal control of the targeted supramolecular aggregates.[8] In particular, the I···N and Br···N intermolecular interactions observed between halogen atoms in diiodo- and dibromoperfluorocarbons and bidentate electron donors such as aliphatic diamines or dipyridyl derivatives has been extensively documented and used to build a variety of supramolecular architectures.[9] In these structures, the presence of fluorine atoms on the organic residue bonded to the halogen plays a key role in dramatically increasing the electron-acceptor ability of the halogen itself.

Theoretical analysis of the nature of halogen bonding showed the primarily electrostatic character of this interaction,[4,10,11] though second-order contributions, such as polarization, dispersion, and charge transfer, have been demonstrated to be nonnegligible.[10] The physical origin of such interaction has been explained[4,11] as due to the presence of a region of positive electrostatic potential localized along the extension of the C−X (X = I, Br, Cl) covalent bond, pointing outward the halogenated molecule. This positive region, later named σ-hole,[12] allows a close approach by an incoming Lewis base, so accounting for both the occurrence and the directionality of halogen bonding.

Other recent investigations[13−15] evidenced that charge transfer, that is, the electron density transfer from the lone pair of the Lewis base to the C−X σ^* antibonding orbital or to outer portions of the halogenated molecule, can be in some cases competitive with the electrostatic contribution. Following the models proposed by Hermansson[16] and Qian and Krimm[17] for hydrogen bonds, the direction and relative weight of the derivatives of the permanent and the induced dipole moments of the halogenated molecule with respect to the C−X bond length have been invoked to explain the occurrence of red-shift rather than blue-shift halogen bonds.[12c]

As a continuation of our charge density studies on halogen-bonded systems,[18,19] in this paper we describe the nature of the Br···N halogen bonding, as well as of other interactions, in the complexes of 1,4-dibromotetrafluorobenzene ($C_6F_4Br_2$) with two dipyridyl derivatives, that is, (*E*)-1,2-bis(4-pyridyl)ethylene (bpe), bpe·$C_6F_4Br_2$, or 4,4′-dipyridyl (dp), dp·$C_6F_4Br_2$, as derived from the X-ray multipole-refined electron density[20] and from DFT calculations. The results of accurate DFT and MP2 evaluations of the interaction energies associated with the corresponding gas-phase halogen bonded dimers will be also reported. Two complexes have been taken into consideration, in this study, in order to draw more reliable conclusions about the relatively weak Br···N interaction, in particular if compared with the stronger I···N halogen bond. The features of the Br···N halogen bond will be compared with those of the previous investigated I···N interaction in the complex of 1,4-diiodotetrafluorobenzene ($C_6F_4I_2$) with bpe, bpe·$C_6F_4I_2$,[18] which

[†] E-mail: a.forni@istm.cnr.it.

10.1021/jp8107182 CCC: $40.75
Published on Web 03/12/2009

TABLE 1: Crystal Data for bpe·$C_6F_4Br_2$ and dp·$C_6F_4Br_2$

	bpe·$C_6F_4Br_2$	dp·$C_6F_4Br_2$
chemical formula	$C_{18}H_{10}Br_2F_4N_2$	$C_{32}H_{16}Br_4F_8N_4$
chemical moieties	$(C_{12}H_{10}N_2 \cdot C_6Br_2F_4)$	$2(C_{10}H_8N_2 \cdot C_6Br_2F_4)$
formula weight	490.10	928.12
dimensions (mm^3)	0.22 × 0.19 × 0.10	0.38 × 0.18 × 0.11
color, habit	colorless, prism	colorless, prism
crystal system	triclinic	triclinic
space group	$P\bar{1}$	$P\bar{1}$
a (Å)	6.0354(12)	5.7691(9)
b (Å)	6.8041(14)	10.8851(15)
c (Å)	11.076(2)	12.1299(15)
α (deg)	83.141(10)	82.698(12)
β (deg)	86.460(10)	82.043(12)
γ (deg)	68.624(10)	82.377(12)
V (Å^3)	420.44(14)	743.12(18)
Z	1	1
ρ_{calcd} (g cm^{-3})	1.936	2.074
μ (mm^{-1})	4.866	5.500
λ (Å), Mo Kα	0.71073	0.71073
scan method	ϕ and ω	ϕ and ω
T (K)	90(2)	90(2)
h,k,l range	−14→14,−16→16, −26→26	−13→13,−25→26, −29→29
$2\theta_{max}$ (deg)	119.80	119.66
no. of measured reflns	57189	153770
no. of independent reflns	12262	21587
R_{int}	0.0312	0.0286
intensity decay	0.00	0.00
absorption correction	multiscan	multiscan
transmission factors T_{min}, T_{max}	0.756, 1.000	0.658, 1.000

is isomorphous with bpe·$C_6F_4Br_2$. The nature of the C−Br bond will be as well discussed and compared with both the other typical covalent bonds of the present structures and the previously investigated C−I bond.[18,19]

2. Methods

X-ray Data Collection. The synthesis and crystals preparation of complexes bpe·$C_6F_4Br_2$ and dp·$C_6F_4Br_2$b were reported elsewhere.[9a] The crystals used for data collection were glued on a glass fiber by perfluorinated oil and slowly cooled to 90 K by a Kryoflex Bruker N_2 gas stream cooling device. X-ray data were collected on a Bruker Smart Apex CCD area detector, and data reduction was made using SAINT programs; absorption corrections based on multiscan were obtained by SADABS. A summary of experimental details is reported in Table 1.

Spherical Atom and Multipole Refinement. The refinements, based on $|F_o|^2$, were performed with the VALTOPO program.[21] The results obtained with the conventional independent atom model (IAM), the same model with inclusion of the third and fourth-order Gram−Charlier terms on the Br atom (IAM+CUM), and the multipole model (POP+CUM) are summarized in Table 2. Atomic and anomalous scattering factors were taken from *International Tables for Crystallography* (1995, Vol. C).

In the POP+CUM multipole refinement, atomic positions, anisotropic thermal and population parameters of Br, F, N, and C pseudoatoms, and third- and fourth-order Gram−Charlier coefficients on the bromine atom were varied. H-atoms positions were kept fixed in the positions obtained by a previous multipole refinement where the H-atoms were polarized in the direction of the atom to which they are bonded, and only their isotropic thermal parameters were refined. To each H atom a radial monopole function $\exp(-2.48r)$ was attributed. The core and the spherical valence density for the other atoms were calculated from Hartree−Fock wave functions.[22] For the deformation density terms, single Slater-type functions with theory-based fixed exponents were used.[23] The expansions over the spherical harmonics were truncated at the hexadecapole level for the bromine atom, octopole level for nitrogen and carbon atoms, quadrupole level for fluorine atoms, and dipole level for the hydrogen atoms. A single parameter was refined for the core of all F, N, and C atoms.

The importance of including in the refinement anharmonic parameters on bromine atoms, which is evident from comparison of the refinement results from IAM and IAM+CUM models (see Table 2), was also tested by excluding these terms from the POP+CUM model. All statistical indices, residual maps, and topological properties at bond critical points indicated that the POP multipole model does not lead to a significant improvement with respect to the POP+CUM best model.

Computational Details. Theoretical analysis of the complex bpe·$C_6F_4Br_2$ has been carried out by performing DFT and MP2 calculations on both the isolated monomers and the halogen-bonded dimer, using Gaussian03.[24] For DFT calculations, the B3LYP[25,26] functional has been used. Several basis sets have been tested, aimed at both reproducing as better as possible the experimental intramolecular geometry and reducing the basis set superposition error. A list of the basis sets used is shown in Table 7, where the reported interaction energies were corrected with the standard counterpoise method.[27] The best results have been obtained at the B3LYP/6-311++G** level of theory. The corresponding electron density distribution has been therefore chosen for topological analysis, which was performed with the AIMPAC program.[28] The same B3LYP/6-311++G** approach has been used for the determination of atomic charges of both complexes bpe·$C_6F_4Br_2$ and dp·$C_6F_4Br_2$.

Periodic DFT calculations at the experimental geometries have been carried out on bpe·$C_6F_4Br_2$ and dp·$C_6F_4Br_2$ with the Crystal98 program,[29] using the same functional as in the gas-phase calculations and the 3-21G* basis set. The topological analysis of the electron density obtained by these calculations was performed with the Topond98 program.[30] This approach was deemed appropriated for the study of the intermolecular interactions in the crystal.

TABLE 2: IAM and Multipole Refinement Information

	bpe·$C_6F_4Br_2$			dp·$C_6F_4Br_2$		
	IAM	IAM+CUM	POP+CUM	IAM	IAM+CUM	POP+CUM
reflections with $\|F_o\|^2 > 0$		11612			19251	
no. of parameters	138	163	372	249	299	684
$R(F)$	0.0345	0.0339	0.0299	0.0386	0.0381	0.0346
$wR(F)$	0.0296	0.0290	0.0237	0.0253	0.0243	0.0198
$R(F^2)$	0.0405	0.0386	0.0301	0.0379	0.0349	0.0274
$wR(F^2)$	0.0575	0.0563	0.0454	0.0490	0.0472	0.0381
S	1.217	1.193	0.971	1.306	1.260	1.027
k (scale factor)	1.004(1)	1.009(1)	1.045(3)	1.006(1)	1.014(1)	1.034(2)
$(shift/esd)_{max}$	<0.01	<0.01	<0.01	<0.01	<0.01	<0.01

TABLE 3: Experimental and Theoretical Bond Lengths and Bond Critical Point and Ring Critical Point Properties of bpe·$C_6F_4Br_2$[a]

X−Y	R_e/Å	R_x/R_e	ρ_{BCP}/e Å^{-3}	$\nabla^2\rho_{BCP}$/e Å^{-5}	λ_1/e Å^{-5}	λ_2/e Å^{-5}	λ_3/e Å^{-5}
C7−Br	1.8749(5)	0.44	1.17(2)	−0.76(33)	−6.3(2)	−5.1(2)	10.7(3)
	1.8977	*0.48*	*1.08*	*−2.88*	*−5.0*	*−4.7*	*6.9*
C7−C8	1.3908(8)	0.47	2.08(4)	−17.4(10)	−16.5(6)	−13.1(6)	12.2(3)
	1.3925	*0.49*	*2.10*	*−20.7*	*−16.2*	*−12.4*	*7.9*
C7−C9	1.3880(8)	0.49	2.12(4)	−17.9(10)	−17.6(5)	−13.3(5)	13.0(3)
	1.3925	*0.49*	*2.10*	*−20.7*	*−16.2*	*−12.4*	*7.9*
C8−C9^{I}	1.3874(7)	0.50	2.22(3)	−19.6(10)	−19.4(5)	−13.6(5)	13.3(3)
	1.3898	*0.50*	*2.14*	*−21.7*	*−17.3*	*−12.5*	*8.0*
C8−F1	1.3333(8)	0.40	1.92(5)	−16.1(21)	−16.6(9)	−13.5(9)	14.1(6)
	1.3381	*0.33*	*1.76*	*3.7*	*−12.0*	*−11.8*	*27.5*
C9−F2	1.3343(9)	0.41	1.92(5)	−14.8(20)	−15.5(9)	−14.6(9)	15.3(6)
	1.3382	*0.33*	*1.76*	*3.7*	*−12.0*	*−11.8*	*27.5*
C1−C1^{II}	1.3460(7)	0.50	2.28(5)	−19.7(15)	−19.3(9)	−13.5(8)	13.1(5)
	1.3444	*0.50*	*2.27*	*−23.8*	*−17.4*	*−13.4*	*7.0*
C1−C2	1.4624(7)	0.52	1.88(3)	−13.2(8)	−14.5(5)	−12.4(4)	13.7(3)
	1.4648	*0.50*	*1.84*	*−16.8*	*−13.2*	*−12.1*	*8.5*
C2−C3	1.4011(8)	0.51	2.06(3)	−16.0(9)	−15.6(5)	−13.2(5)	13.2(3)
	1.4047	*0.51*	*2.05*	*−20.1*	*−15.2*	*−12.9*	*8.0*
C2−C6	1.3988(8)	0.49	2.09(4)	−17.2(9)	−16.5(5)	−13.7(5)	13.0(3)
	1.4027	*0.51*	*2.06*	*−20.4*	*−15.4*	*−13.0*	*8.0*
C3−C4	1.3881(8)	0.50	2.12(4)	−15.9(10)	−16.3(6)	−13.2(5)	13.6(3)
	1.3877	*0.50*	*2.12*	*−21.3*	*−16.1*	*−13.1*	*7.8*
C6−C5	1.3891(8)	0.50	2.11(4)	−16.8(10)	−17.0(6)	−13.2(5)	13.3(3)
	1.3909	*0.50*	*2.11*	*−21.3*	*−16.0*	*−13.2*	*7.9*
C4−N	1.3413(9)	0.46	2.35(4)	−16.7(14)	−18.5(7)	−17.3(7)	19.1(5)
	1.3398	*0.37*	*2.28*	*−23.4*	*−17.4*	*−15.8*	*9.9*
C5−N	1.3367(10)	0.44	2.28(5)	−18.1(17)	−18.4(8)	−16.1(8)	16.3(5)
	1.3358	*0.37*	*2.30*	*−23.3*	*−17.6*	*−15.9*	*10.2*
C1−H1	1.01(2)	0.57	2.00(6)	−22.4(17)	−18.2(9)	−16.7(9)	12.5(7)
	1.086	*0.64*	*1.90*	*−23.2*	*−18.0*	*−17.7*	*12.5*
C3−H3	1.05(2)	0.60	1.92(5)	−17.9(14)	−17.8(8)	−16.3(8)	16.1(6)
	1.083	*0.64*	*1.90*	*−23.4*	*−18.1*	*−17.8*	*12.5*
C4−H4	1.07(2)	0.63	1.87(6)	−16.1(13)	−17.3(8)	−16.9(8)	18.1(6)
	1.086	*0.65*	*1.93*	*−24.1*	*−18.9*	*−18.4*	*13.1*
C5−H5	1.05(2)	0.62	1.88(5)	−16.0(14)	−17.6(8)	−16.3(8)	17.8(6)
	1.086	*0.65*	*1.93*	*−24.1*	*−18.9*	*−18.4*	*13.1*
C6−H6	1.06(2)	0.62	1.88(5)	−16.9(12)	−17.9(7)	−16.2(7)	17.2(6)
	1.084	*0.64*	*1.90*	*−23.2*	*−18.1*	*−17.7*	*12.5*
C7−C8−C9^{I}−C7^{I}−C8^{I}−C9			0.206(7)	2.78(5)	−0.34(4)	1.42(9)	1.70(8)
			0.134	*3.54*	*−0.32*	*1.91*	*1.95*
C2−C3−C4−N−C5−C6			0.254(5)	3.26(4)	−0.62(3)	1.81(6)	2.08(7)
			0.161	*4.16*	*−0.48*	*2.10*	*2.54*

[a] R_e = distance between atoms X and Y; R_x = distance between atom X and the BCP. First row: experimental POP+CUM model; second row: theoretical B3LYP/6-311++G** calculations on the isolated dimer at the geometry optimized at the same level of theory. The Roman numerals refer to the following symmetry operations: I: $3-x, -2-y, -1-z$; II: $-x, -y, -z$.

Evaluation of Atomic Charges. Atomic charges have been obtained by integration of electron density over the topological atomic basins Ω, according to the Bader's quantum theory of atoms in molecules (QTAIM).[31] The accuracy of integration has been estimated through evaluation of the integrated number of electrons (N_Ω), volume (V_Ω), and Laplacian (L_Ω). The corresponding errors, $N_{err}(\%) = (\sum_\Omega m_\Omega N_\Omega - N_{cell})/N_{cell}$; $V_{err}(\%) = (\sum_\Omega m_\Omega V_\Omega - V_{cell})/V_{cell}$; $L_{err} = (\sum_\Omega L^2_\Omega/N_{atoms})^{1/2}$, where m_Ω is the site multiplicity for atom Ω, were evaluated for both the theoretical and the X-ray derived charge distribution. They were negligible for the former, while for the latter we obtained $N_{err}(\%) = 0.004, 0.04$; $V_{err}(\%) = 0.16, 0.12$; $L_{err} = 0.016, 0.021$ e Å^{-2}, for bpe·$C_6F_4Br_2$ and dp·$C_6F_4Br_2$, respectively. These errors are of the same order of magnitude of those previously estimated for smaller systems such as alanine[21] and for the complex bpe·$C_6F_4I_2$,[21] and are indicative of the significance of the specific values of atomic charges. In particular, for dp·$C_6F_4Br_2$ the $N_{err}(\%)$ value corresponds to a defect of 0.08 e on the asymmetric unit, which comprises two half-dimers of dp·$C_6F_4Br_2$ (see below).

3. Results and Discussion

The structural details of bpe·$C_6F_4Br_2$ and dp·$C_6F_4Br_2$ have been discussed in a previous paper.[9a] Bond distances and selected intermolecular contacts (approximately within the sum of the van der Waals radii[32]) from the final multipole refinement (POP+CUM) are reported respectively in Tables 3 and 5 for bpe·$C_6F_4Br_2$, and Tables 4 and 6 for dp·$C_6F_4Br_2$.

The unit cell of bpe·$C_6F_4Br_2$ consists of one bpe and one $C_6F_4Br_2$ molecule, both lying on a center of symmetry. They are connected to each other through Br···N halogen bonds forming 1:1 infinite chains (see Figure 1). Parallel halogen-bonded chains are linked by H1···F2$_{2-x,-1-y,-z}$, H3···F1$_{1-x,-1-y,-1-z}$ and H6···F2$_{2-x,-1-y,-z}$ hydrogen bonds, forming slightly corrugated molecular planes. These planes are connected to each other by the H4···F2$_{-1+x,y,z}$ hydrogen bond and by $\pi-\pi$ interactions involving bispyridyl and dibromotetrafluorobenzene molecules. The crystal structure of bpe·$C_6F_4Br_2$ is then isomorphous to that of the previously investigated analogous iodine complex, bpe·$C_6F_4I_2$.[18] In

TABLE 4: Experimental Bond Lengths and Bond Critical Point and Ring Critical Point Properties of dp·$C_6F_4Br_2$[a]

X−Y	R_e/Å	R_x/R_e	ρ_{BCP}/e Å^{-3}	$\nabla^2\rho_{BCP}$/e Å^{-5}	λ_1/e Å^{-5}	λ_2/e Å^{-5}	λ_3/e Å^{-5}
C7−Br	1.8700(7)	0.45	1.20(2)	−0.27(31)	−5.9(2)	−5.8(2)	11.4(3)
	1.8722(7)	0.45	1.18(3)	−0.65(54)	−6.5(2)	−5.4(5)	11.3(3)
C7−C8	1.3882(8)	0.49	2.13(3)	−17.8(9)	−17.1(5)	−13.7(5)	13.0(2)
	1.3887(8)	0.51	2.12(5)	−18.9(11)	−18.1(6)	−13.4(7)	12.6(2)
C7−C9	1.3906(8)	0.49	2.17(3)	−17.5(9)	−17.7(5)	−13.5(5)	13.7(2)
	1.3888(8)	0.50	2.18(2)	−18.3(2)	−17.9(4)	−13.8(2)	13.5(1)
C8−C9^{I,II}	1.3865(9)	0.50	2.27(3)	−20.2(9)	−19.8(5)	−14.1(5)	13.6(2)
	1.3877(9)	0.51	2.17(2)	−19.4(3)	−19.0(2)	−13.5(2)	13.1(1)
C8−F1	1.3349(9)	0.41	2.04(5)	−17.1(19)	−17.5(9)	−16.0(9)	16.4(6)
	1.3295(9)	0.40	2.06(1)	−19.2(3)	−18.1(2)	−16.6(2)	15.6(4)
C9−F2	1.3334(9)	0.40	2.05(5)	−18.7(20)	−17.4(9)	−16.6(9)	15.3(6)
	1.3324(9)	0.40	1.93(2)	−15.8(7)	−15.8(3)	−15.0(4)	15.0(5)
C2−C2^{III,IV}	1.4816(9)	0.50	1.80(4)	−11.1(9)	−13.4(6)	−11.4(5)	13.8(3)
	1.4827(9)	0.50	1.86(4)	−13.4(9)	−14.2(6)	−12.9(5)	13.7(3)
C2−C3	1.3977(8)	0.50	2.11(3)	−15.8(8)	−16.4(5)	−13.1(5)	13.7(2)
	1.3979(10)	0.50	2.11(4)	−17.4(8)	−17.0(5)	−13.7(5)	13.2(2)
C2−C6	1.3989(10)	0.51	2.02(3)	−15.9(9)	−15.6(5)	−12.6(5)	12.4(2)
	1.3997(8)	0.50	2.06(24)	−16.3(73)	−16.0(40)	−13.2(33)	13.0(3)
C3−C4	1.3891(11)	0.48	2.22(3)	−19.8(9)	−18.3(5)	−14.6(5)	13.2(2)
	1.3896(11)	0.48	2.19(3)	−20.1(7)	−17.8(4)	−15.0(3)	12.7(3)
C6−C5	1.3890(11)	0.49	2.15(3)	−18.4(9)	−17.5(5)	−14.1(5)	13.3(2)
	1.3914(10)	0.49	2.19(1)	−18.6(39)	−17.8(35)	−14.4(17)	13.6(4)
C4−N	1.3369(11)	0.44	2.34(4)	−20.6(16)	−20.1(7)	−16.8(7)	16.3(5)
	1.3366(10)	0.42	2.29(5)	−21.4(17)	−19.2(8)	−16.5(8)	14.2(5)
C5−N	1.3381(10)	0.45	2.31(4)	−18.1(16)	−18.3(7)	−17.2(7)	17.4(5)
	1.3406(11)	0.46	2.40(5)	−19.0(10)	−20.1(7)	−17.7(7)	18.7(5)
C3−H3	1.073(18)	0.63	1.80(5)	−14.5(11)	−16.7(6)	−16.0(6)	18.2(5)
	1.087(20)	0.66	1.79(2)	−14.1(5)	−17.9(3)	−16.5(3)	20.4(3)
C4−H4	1.072(18)	0.66	1.98(6)	−18.5(14)	−20.5(8)	−18.7(8)	20.8(6)
	1.106(20)	0.66	1.80(5)	−14.8(12)	−17.9(6)	−16.8(6)	19.9(3)
C5−H5	1.081(18)	0.65	1.80(4)	−14.6(11)	−17.5(6)	−16.5(6)	19.3(5)
	1.062(18)	0.64	1.89(2)	−18.3(4)	−18.8(3)	−17.6(3)	18.1(2)
C6−H6	1.092(18)	0.65	1.80(12)	−13.8(12)	−17.5(7)	−16.5(7)	20.2(5)
	1.070(19)	0.65	1.89(20)	−16.7(63)	−18.7(34)	−17.7(30)	19.7(3)
C7−C8−C9^{I,II}−C7^{I,II}−C8^{I,II}−C9			0.21(1)	2.88(5)	−0.33(4)	1.39(8)	1.82(8)
			0.20(1)	2.75(4)	−0.30(5)	1.24(5)	1.81(6)
C2−C3−C4−N−C5-C6			0.24(1)	3.24(4)	−0.56(3)	1.75(7)	2.06(7)
			0.25(2)	3.31(9)	−0.59(11)	1.77(13)	2.13(25)

[a] R_e = distance between atoms X and Y; R_x = distance between atom X and the bcp. First row: molecule a, second row: molecule b. The Roman numerals refer to the following symmetry operations: I: $-x, -y, -z$; II: $1-x, 2-y, 1-z$; III: $1-x, 1-y, 1-z$; IV: $-x, 1-y, -z$. Operations I,III and II,IV apply to molecules a and b, respectively.

particular, the pattern of intermolecular interactions in the two structures is essentially the same within layers, but slightly different among layers.

The unit cell of dp·$C_6F_4Br_2$ is formed by two molecules (a and b) of dp and two molecules (a and b) of $C_6F_4Br_2$. The four molecules lie on four different centers of symmetry and are connected two by two through Br···N halogen bonds forming two distinct and parallel 1:1 infinite chains (see Figure 2). The modules involved in both chains are not coplanar, and the dihedral angle between the least-squares planes through dp and $C_6F_4Br_2$ heavy atoms is 61(1) and 60(1)° for the dimers a and b, respectively.

The final difference Fourier maps ($F_{observed} - F_{multipole}$), given as Supporting Information, are featureless and the largest peaks, close to bromine, are 0.17(3) and 0.22(2) e Å^{-3} for bpe·$C_6F_4Br_2$ and dp·$C_6F_4Br_2$, respectively. The observed deformation maps ($F_{observed} - F_{IAM}$), see Figure 3 for bpe·$C_6F_4Br_2$ and Supporting Information for dp·$C_6F_4Br_2$, show bonding density in every C−Br, C−C, C−N, and C−H bond. As expected, for the polar C−F bonds a very low bonding density accumulation is observed. Density accumulation is evident around F and Br atoms, associated with their lone pairs, and in the direction of the Br···N intermolecular bond.

Topological Analysis of Electron Density. The electron density, $\rho(\mathbf{r})$, and its Laplacian, $\nabla^2\rho(\mathbf{r})$, were analyzed by the quantum theory of atoms in molecules (QTAIM).[31] The properties of the experimental POP+CUM electron density at the bond critical points (BCP's) of bpe·$C_6F_4Br_2$ and dp·$C_6F_4Br_2$ are reported in Tables 3 and 4, respectively. For the former complex, the corresponding theoretical B3LYP/6-311++G** values are also reported in Table 3. Figures 4 and 5 show the experimental Laplacian maps of the two complexes.

The topological features of corresponding bonds in the two structures are generally reproduced within 3 times the standard uncertainties. In particular, the C7−Br bonds are characterized by very similar values of BCP properties (ρ_{BCP} and $\nabla^2\rho_{BCP}$ are, on average, 1.18(2) e Å^{-3} and −0.6(4) e Å^{-5}, respectively). The slightly negative value of Laplacian indicates a very low covalence degree for this interaction, compared with the other bonds of the present structures (see $\nabla^2\rho_{BCP}$ values of Tables 3, 4 and Figures 4, 5). On the other hand, the C−Br bond is well distinguishable from the C−I bond, as investigated in the analogous iodine complex bpe·$C_6F_4I_2$[18] and in the complex of $C_6F_4I_2$ with 4,4′-dipyridyl-*N*,*N*′-dioxide, dpNO·$C_6F_4I_2$.[19] For the latter bond, the average values of ρ_{BCP} and $\nabla^2\rho_{BCP}$ are 0.75(2) e Å^{-3} and 1.8(2) e Å^{-5}, respectively, where the slightly positive Laplacian is indicative of closed-shell character for the C−I bond.

The two carbon−halogen bonds can be better discriminated by looking at the BCP curvatures λ_i, which are significantly

TABLE 5: Contact Geometry and Experimental and Theoretical Bond Critical Point Properties of Intermolecular Interactions in bpe·$C_6F_4Br_2$[a]

X···Y	R_e/Å	C−X···Y/deg	R_x/R_e	ρ_{BCP}/e Å^{-3}	$\nabla^2\rho_{BCP}$/e Å^{-5}	G_{BCP}/hartrees Å^{-3}	V_{BCP}/hartrees Å^{-3}	H_{BCP}/ρ_{BCP}	$\lvert V_{BCP}\rvert/G_{BCP}$
				Halogen Bond					
Br···N	2.8219(6)	179.18(2)	0.54	0.183(2)	2.08(3)	0.145(2)	−0.144(4)	0.005(4)	0.993(4)
			0.50	*0.148*	*1.70*	*0.117*	*−0.115*	*0.016*	*0.979*
	2.9455	*178.95*	*0.51*	*0.113*	*1.25*	*0.078*	*−0.068*	*0.090*	*0.87*
				Hydrogen Bonds					
H3···F1^{I}	2.41(2)	128(1)	0.45	0.055(4)	0.99(2)	0.052(1)	−0.036(3)	0.31(1)	0.68(1)
			0.43	*0.052*	*1.26*	*0.064*	*−0.041*	*0.46*	*0.63*
H1···F2^{II}	2.52(2)	161(1)	0.43	0.030(5)	0.68(2)	0.034(1)	−0.020(3)	0.45(2)	0.60(1)
			0.43	*0.033*	*0.86*	*0.041*	*−0.021*	*0.59*	*0.52*
H6···F2^{II}	2.76(2)	145(1)	0.45	0.018(2)	0.35(2)	0.017(1)	−0.010(2)	0.41(2)	0.58(2)
			0.45	*0.017*	*0.44*	*0.019*	*−0.008*	*0.70*	*0.39*
H4···F2^{III}	3.14(2)	102(1)	0.51	0.017(1)	0.27(1)	0.014(1)	−0.008(1)	0.31(1)	0.60(1)
			0.51	*0.010*	*0.29*	*0.014*	*−0.007*	*0.68*	*0.48*
				Hydrogen−Hydrogen Bonds					
H5···H5^{II}	2.17(3)		0.50	0.038(8)	0.70(4)	0.036(2)	−0.023(5)	0.34(3)	0.64(2)
			0.50	*0.043*	*0.79*	*0.038*	*−0.022*	*0.39*	*0.57*
H3···H5^{III}	2.57(2)		0.51	0.035(3)	0.48(2)	0.025(1)	−0.017(2)	0.24(1)	0.68(1)
			0.51	*0.030*	*0.43*	*0.022*	*−0.014*	*0.27*	*0.64*
H6···H6^{IV}	3.00(2)		0.50	0.038(2)	0.44(2)	0.024(1)	−0.017(2)	0.18(1)	0.72(1)
			0.50	*0.034*	*0.43*	*0.024*	*−0.020*	*0.11*	*0.84*
				$\pi-\pi$ Interactions					
C4···C9^{V}	3.2925(10)		0.50	0.050(1)	0.53(1)	0.030(1)	−0.023(1)	0.141(5)	0.768(7)
			0.50	*0.048*	*0.47*	*0.031*	*−0.029*	*0.044*	*0.932*
C2···C5^{VI}	3.3664(9)		0.52	0.046(1)	0.50(1)	0.028(1)	−0.021(1)	0.149(4)	0.754(6)
			0.53	*0.047*	*0.48*	*0.031*	*−0.029*	*0.043*	*0.936*
				Other Interactions					
Br···F1^{VII}	3.4939(8)		0.57	0.033(1)	0.48(1)	0.025(1)	−0.017(1)	0.257(2)	0.662(2)
			0.57	*0.024*	*0.57*	*0.029*	*−0.017*	*0.476*	*0.608*
Br···F2^{III}	3.5957(9)		0.57	0.026(1)	0.38(1)	0.019(1)	−0.012(1)	0.270(2)	0.640(2)
			0.57	*0.018*	*0.46*	*0.023*	*−0.013*	*0.541*	*0.570*
F1···F1^{VIII}	2.8845(10)		0.50	0.046(1)	0.86(1)	0.045(1)	−0.030(1)	0.328(4)	0.661(3)
			0.50	*0.031*	*1.20*	*0.059*	*−0.035*	*0.784*	*0.589*

[a] First row: experimental POP+CUM model; second row: periodic B3LYP/3-21G* calculations at the experimental geometry; third row (only for the halogen bond): theoretical B3LYP/6-311++G** calculations on the isolated dimer optimized on the BSSE free potential energy surface. The Roman numerals refer to the following symmetry operations: I: $1-x, -1-y, -1-z$; II: $2-x, -1-y, -z$; III: $-1+x, y, z$; IV: $1-x, -y, -z$; V: $-1+x, 1+y, z$; VI: $1-x, -1-y, -z$; VII: $2-x, -1-y, -1-z$; VIII: $2-x, -2-y, -1-z$.

larger for the C−Br with respect to the C−I bond. In particular, the curvature along the bond direction for C−Br, λ_3, is of the same order of magnitude as the other covalent bonds. This difference denotes a more structured electron density distribution around bromine with respect to iodine. This information can be further evidenced by examining the topology of the Laplacian $\nabla^2\rho(\mathbf{r})$ around the two halogen atoms. A search of its critical points (ω,σ) was performed for the bpe·$C_6F_4Br_2$ complex, ω being the number of nonzero eigenvalues of the Hessian matrix associated with $\nabla^2\rho(\mathbf{r})$, and σ the number of positive eigenvalues minus the number of the negative ones. In particular, we were interested in the search of the (3,+3) critical points in the valence shell charge concentration (VSCC) region, that is, the points of local minimum in the outer atomic shell region with $\nabla^2\rho(\mathbf{r}) < 0$, where the electron density is locally concentrated. Similarly to what obtained for the analogous iodine complex,[18] four (3,+3) critical points were found in the VSCC region around the halogen atom, located far from the directions of the intra- and intermolecular interactions. They are clearly visible in Figure 4, and only three of them are visible in Figure 5b.[33] A comparison between the values assumed by the topological properties at the (3,+3) Laplacian critical points around bromine and iodine (on average, $\nabla^2\rho = -9.4$ and -0.4 e Å^{-5}; $\rho = 1.53$ and 0.63 e Å^{-3} for Br and I, respectively) indicates a much flatter distribution of electron density around iodine with respect to bromine, in agreement with what is envisaged by the curvatures at the BCPs (see Figure S3 in Supporting Information for a direct comparison between the bromine and the iodine complexes). Moreover, the Laplacian critical points are located significantly closer to the nucleus in bromine with respect to iodine (0.777 and 1.081 Å on average for Br and I, respectively), taking also into account the difference of their van der Waals radii (0.304 Å versus $\Delta r(\mathrm{vdW}) = 0.13$ Å).

The VSCC associated with the carbon bonded to the halogen atom shows as well slight differences in the two structures. The (3,+3) critical point directed toward the halogen nucleus (see Figures 4 and 5a) is placed at 0.478 Å ($\rho = 1.75$ e Å^{-3}, $\nabla^2\rho = -25.1$ e Å^{-5} at the Laplacian critical point) for $C_6F_4Br_2$, and at 0.465 Å ($\rho = 2.00$ e Å^{-3}, $\nabla^2\rho = -35.7$ e Å^{-5} at the Laplacian critical point) for $C_6F_4I_2$, in agreement with the greater covalence degree of the C−Br with respect to the C−I bond. Less significant differences are observed in the VSCC associated with the N atom in the direction of the halogen atoms. In this case, the Laplacian critical points are placed in both structures at 0.390 Å from the N nucleus, with ρ and $\nabla^2\rho$ values equal to 3.83 e Å^{-3} and −79.9 e Å^{-5} for $C_6F_4Br_2$, and 3.93 e Å^{-3} and −86.3 e Å^{-5} for $C_6F_4I_2$.

Chemical bonds can be further characterized by the local electron energy density, $H_{BCP} = G_{BCP} + V_{BCP}$,[34] G_{BCP} and V_{BCP} being respectively the values of the local kinetic and potential energy density at the BCP, which can be estimated through Abramov's approximation.[35,36] As suggested by Espinosa et al.,[37]

TABLE 6: Contact Geometry and Experimental and Theoretical Bond Critical Point Properties of Selected Intermolecular Interactions in dp·$C_6F_4Br_2$[a,b]

X···Y	R_e/Å	C−X···Y/deg	R_x/R_e	ρ_{BCP}/e Å^{-3}	$\nabla^2\rho_{BCP}$/e Å^{-5}	G_{BCP}/hartrees Å^{-3}	V_{BCP}/hartrees Å^{-3}	H_{BCP}/ρ_{BCP}	$\lvert V_{BCP}\rvert/G_{BCP}$
				Halogen Bonds					
Br_a···N_a	2.8800(9)	177.22(4)	0.54	0.156(2)	1.86(2)	0.123(1)	−0.117(3)	0.045(3)	0.943(4)
			0.50	*0.128*	*1.54*	*0.102*	*−0.097*	*0.040*	*0.950*
Br_b···N_b	2.9785(9)	176.25(3)	0.54	0.123(1)	1.47(2)	0.093(1)	−0.083(3)	0.081(4)	0.893(4)
			0.50	*0.104*	*1.28*	*0.082*	*−0.074*	*0.076*	*0.904*
				Hydrogen Bonds					
H5_a···F2_b^{I}	2.33(2)	159(1)	0.41	0.043(6)	1.02(2)	0.052(1)	−0.032(3)	0.45(2)	0.62(1)
			0.42	*0.059*	*1.40*	*0.074*	*−0.049*	*0.42*	*0.67*
H4_a···F2_a^{II}	2.47(2)	135(1)	0.44	0.041(4)	0.80(2)	0.041(1)	−0.026(2)	0.36(2)	0.64(1)
			0.43	*0.041*	*1.05*	*0.052*	*−0.030*	*0.53*	*0.58*
H5_b···F1_b^{III}	2.51(2)	133(1)	0.44	0.037(1)	0.70(1)	0.036(1)	−0.023(1)	0.36(1)	0.64(1)
			0.43	*0.037*	*0.96*	*0.046*	*−0.026*	*0.56*	*0.56*
H5_b···F1_a^{IV}	2.59(2)	128(1)	0.45	0.030(1)	0.56(1)	0.029(1)	−0.018(1)	0.35(1)	0.63(1)
			0.44	*0.027*	*0.75*	*0.036*	*−0.018*	*0.63*	*0.52*
H4_b···C4_a	2.74(2)	130(1)	0.38	0.050(3)	0.70(2)	0.038(1)	−0.027(2)	0.22(1)	0.72(1)
			0.37	*0.062*	*0.80*	*0.048*	*−0.040*	*0.13*	*0.83*
H3_a···N_b^{II}	2.75(2)	145(1)	0.42	0.035(3)	0.52(2)	0.027(1)	−0.018(2)	0.26(1)	0.67(1)
			0.40	*0.040*	*0.70*	*0.038*	*−0.026*	*0.29*	*0.69*
H6_a···N_b^{I}	2.81(2)	148(1)	0.41	0.025(3)	0.43(2)	0.022(1)	−0.013(2)	0.34(2)	0.62(1)
			0.40	*0.033*	*0.55*	*0.028*	*−0.017*	*0.33*	*0.62*
H5_b···Br1_b^{III}	3.18(2)	148(1)	0.37	0.022(1)	0.35(1)	0.018(1)	−0.011(1)	0.30(1)	0.62(1)
			0.37	*0.031*	*0.40*	*0.021*	*−0.014*	*0.22*	*0.68*
H4_a···Br1_a^{II}	3.24(2)	142(1)	0.37	0.024(2)	0.34(2)	0.017(1)	−0.011(2)	0.26(1)	0.64(2)
			0.37	*0.028*	*0.36*	*0.018*	*−0.012*	*0.23*	*0.65*
				Hydrogen−Hydrogen Bonds					
H6_a···H6_a^{I}	2.79(2)		0.50	0.023(2)	0.31(2)	0.016(1)	−0.010(2)	0.24(2)	0.64(2)
			0.50	*0.021*	*0.29*	*0.015*	*−0.010*	*0.25*	*0.65*
H3_a···H5_a^{II}	2.84(2)		0.49	0.031(1)	0.38(1)	0.020(1)	−0.014(1)	0.21(1)	0.68(1)
			0.48	*0.027*	*0.34*	*0.019*	*−0.014*	*0.19*	*0.73*
H3_b···H3_b^{V}	2.88(2)		0.50	0.015(1)	0.22(1)	0.011(1)	−0.007(2)	0.28(1)	0.61(1)
			0.50	*0.015*	*0.22*	*0.011*	*−0.006*	*0.28*	*0.60*
H4_b···H6_b^{II}	2.99(2)		0.50	0.025(3)	0.30(4)	0.016(2)	−0.010(4)	0.22(3)	0.66(4)
			0.47	*0.023*	*0.30*	*0.016*	*−0.012*	*0.19*	*0.74*

[a] First row: experimental POP+CUM model; second row: periodic B3LYP/3-21G* calculations at the experimental geometry; the Roman numerals refer to the following symmetry operations: I: $-x, 1-y, 1-z$; II: $1+x, y, z$; III: $-1+x, y, z$; IV: $-1+x, 1+y, z$; V: $1-x, 1-y, -z$. [b] Other interactions reported as Supporting Information.

TABLE 7: Selected Geometrical Parameters (Å) and Interaction Energies ΔE (kcal/mol) for Optimized Gas-Phase Dimers of bpe·$C_6F_4Br_2$ and bpe·$C_6F_4I_2$[a]

	C−X	X···N	ΔE_{uncorr}	$\Delta E_{BSSE\ corr}$	$\Delta E_{BSSE\ free}$
bpe·$C_6F_4Br_2$					
B3LYP/SDD	1.9469	2.7746	5.59	5.17	
MP2/SDD	1.9587	2.7555	7.56	4.77	
B3LYP/MIDI!	1.8924	2.7744	6.86	3.10	
MP2/MIDI!	1.8953	2.7491	8.15	3.56	
B3LYP/6-311++G**	1.8977	2.9343	3.35	3.47	3.22[b]
experimental	1.8749(6)	2.8219(8)			
bpe·$C_6F_4I_2$					
B3LYP/SDD	2.1505	2.7863	8.44	8.01	
MP2/SDD	2.1609	2.7775	10.44	7.65	
B3LYP/MIDI!	2.1176	2.7834	9.67	5.16	5.10[b]
MP2/MIDI!	2.1168	2.7590	11.00	5.25	5.37[b]
experimental[c]	2.0969(7)	2.7804(8)			

[a] Interaction energies computed as difference between the energy of the dimer and the sum of the energies of the single monomers, uncorrected (ΔE_{uncorr}) and corrected for BSSE ($\Delta E_{BSSE\ corr}$), and obtained from optimization on the BSSE free potential energy surface ($\Delta E_{BSSE\ free}$). [b] The halogen bond distances optimized on the BSSE free potential energy surface are Br···N = 2.9455 Å and I···N = 2.8965 (B3LYP), 2.9299 (MP2) Å. [c] Reference 18.

the atomic interactions can be divided in three regions on the basis of the ratio $\lvert V_{BCP}\rvert/G_{BCP}$: *pure* closed shell (region I, $\lvert V_{BCP}\rvert/G_{BCP} < 1$), *transit* closed shell (region II, $1 < \lvert V_{BCP}\rvert/G_{BCP} < 2$), and *pure* shared shell (region III, $\lvert V_{BCP}\rvert/G_{BCP} > 2$). Abramov's approximation largely overestimates both the G_{BCP} and V_{BCP} magnitudes for covalent bonds.[35] However, these errors are widely compensated in calculating H_{BCP} and the ratio $\lvert V_{BCP}\rvert/G_{BCP}$.[19] In region I, according to Espinosa et al.,[37] the (positive) H_{BCP}/ρ_{BCP} parameter indicates the "softening degree" (SD) of the interaction per electron density unity at the BCP: the weaker the interaction, the greater the SD magnitude. In regions II and III, the (negative) H_{BCP}/ρ_{BCP} ratio is a measure of the "covalence degree" (CD) of the interaction: the stronger the interaction, the greater the CD magnitude.

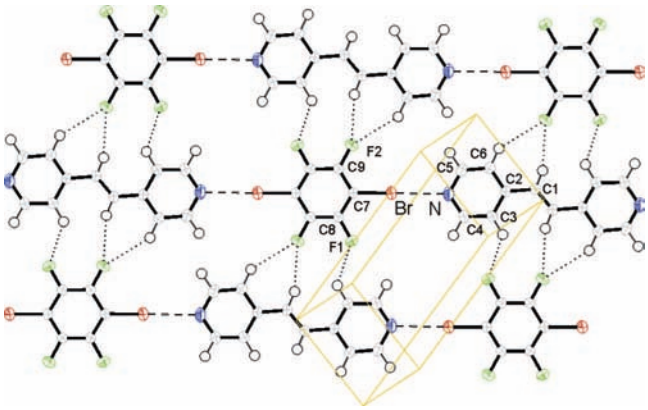

Figure 1. Packing diagram of bpe·$C_6F_4Br_2$ at 90 K with atom numbering scheme. Ellipsoids at 90% probability level.

For the C−Br bond the experimental $|V_{BCP}|/G_{BCP}$ ratios are 2.05(1), 2.02(1), and 2.04(2) for bpe·$C_6F_4Br_2$ and the two nonequivalent dimers of dp·$C_6F_4Br_2$, respectively, so it falls on the borderline between *transit* and *pure* shared shell regions. On the other hand, the C−I bond has $|V_{BCP}|/G_{BCP} = 1.84(2)$[18] and 1.75(2),[19] and it is classified as *transit* closed shell interaction. The H_{BCP}/ρ_{BCP} ratios, −0.91(2) for the C−Br bond in both bromine complexes and −0.63(2), −0.59(2) for the C−I bond in bpe·$C_6F_4I_2$[18] and dpNO·$C_6F_4I_2$,[19] provide a quantitative evaluation of the different covalence degree of the two carbon−halogen bonds. For comparison, all the other bonds in the present structures have H_{BCP}/ρ_{BCP} between −1.33(5) and −1.63(5).

The goodness of Abramov's approximation can be judged by comparing the $|V_{BCP}|/G_{BCP}$ ratios obtained from exact evaluation of V_{BCP} and G_{BCP} by theoretical methods on the optimized halogen-bonded dimers and from the use of the approximated formula on the same wave function. The exact and estimated ratios are respectively $|V_{BCP}|/G_{BCP} = 2.48$ and 2.26 for bpe·$C_6F_4Br_2$ (from B3LYP/6-311++G** calculations); 1.66 and 1.74 for bpe·$C_6F_4I_2$; and 1.83 and 1.87 for dpNO·$C_6F_4I_2$ (both from B3LYP/MIDI! calculations). As expected,[35] the better agreement between the estimated and the exact values is achieved for the less covalent C−I bond.

Intermolecular Interactions. The topological properties of the main intermolecular interactions for bpe·$C_6F_4Br_2$ and dp·$C_6F_4Br_2$ are reported in Tables 5 and 6, respectively. The geometrical and topological features of the Br···N interaction are very similar in the two structures. In complex bpe·$C_6F_4Br_2$, the density and Laplacian BCP values are slightly larger than those of dp·$C_6F_4Br_2$, on account of the shorter distance between the interacting atoms in the former complex. The $|V_{BCP}|/G_{BCP}$ ratios, close to 1, indicate for this interaction a character at the boundary between *pure* and *transit* closed shell regions. This is confirmed by the small and positive values of the H_{BCP}/ρ_{BCP} ratios. For comparison, the I···N halogen bond, though is characterized by a very similar value of Laplacian at BCP, assumes a partial shared-shell character ($H_{BCP}/\rho_{BCP} = -0.11(1)$) and is classified as *transit* closed shell interaction ($|V_{BCP}|/G_{BCP} = 1.16(1)$).

Analysis of the Laplacian distribution around the Br···N and I···N pairs clearly reveals a key−lock arrangement (see Figures 4 and 5), in which a region of charge concentration in the valence shell of the N atom faces a charge depletion region in the valence shell of the halogen atom.[38] This arrangement explains the strong directionality of the halogen-bonding interaction, in full agreement with what expected on the basis of the electrostatic potential distribution of the isolated monomers.[11,12]

Besides the Br···N halogen bond, weak C−H···N, C−H···F, and C−H···Br hydrogen bonds, π/π interactions between aromatic rings (see Table 5, C4···C9 and C2···C5 pairs), and other intermolecular interactions contribute to stabilize the structures. Among them, a number of H···H, F···F and Br···Br interactions between atoms of the same species, similar or identical, have been detected. In particular, intramolecular H···H bonding was previously demonstrated by Matta et al.[39] to make a stabilizing contribution of up to 10 kcal/mol in planar aromatic systems. In the present structures, much weaker H···H interactions are of course to be expected, the atoms being mostly separated by much more the sum of their van der Waals radii. Their physical presence has been, however, detected also by topological analysis of the theoretical charge density distribution (see Tables 5 and 6). The associated H_{BCP}/ρ_{BCP} and $|V_{BCP}|/G_{BCP}$ ratios (on average 0.24 and 0.66, respectively, from both experiment and theory) are very similar to those computed by Matta et al.,[39] while the lower ρ_{BCP} values obtained in the present structures (0.029 e Å^{-3} on average) are indicative of the weakness of such interactions. The F···F interaction observed in bpe·$C_6F_4Br_2$, on the other hand, shows geometrical and topological features almost identical to those reported for the structures of tetrafluorophthalonitrile and tetrafluoroisophthalonitrile.[40] The values of the H_{BCP}/ρ_{BCP} and $|V_{BCP}|/G_{BCP}$ ratios for all these weak intermolecular interactions, falling in the ranges 0.14(1)−0.45(2) and 0.58(2)−0.77(1), respectively, are indicative of *pure* closed shell character, clearly distinguished from the Br···N halogen bond interaction.

In order to compare the relative strength of the different intermolecular interactions, we can use the simple empirical formula proposed by Espinosa et al.[36] for the determination of the energy of hydrogen bonds, $E_{HB} = {}^1/_2 V_{BCP}$. We obtain −6.7(2), −5.4(1), and −3.9(1) kcal/mol for the Br···N halogen bond in bpe·$C_6F_4Br_2$ and the two nonequivalent dimers of dp·$C_6F_4Br_2$, respectively, reflecting the slightly greater stability of this interaction in the former structure. These values are also indicative of the lower strength of the Br···N interaction with respect to the I···N halogen bond, for which the estimated interaction energy in bpe·$C_6F_4I_2$ was −8.5(2) kcal/mol.[18] For the other intermolecular interactions reported in Tables 5 and 6, E_{HB} falls between −1.7(1) and −0.38(3) kcal/mol. A similar range [−2.1(2),−0.56(7) kcal/mol] was obtained for the weak interactions in bpe·$C_6F_4I_2$.[18]

A more accurate evaluation of the X···N (X = Br, I) halogen-bonding energy, based on theoretical approaches, has been carried out for the gas-phase dimers of bpe·$C_6F_4Br_2$ and bpe·$C_6F_4I_2$ by optimizing their geometry at different levels of theory. The results are summarized in Table 7, where the lengths of the C−X bonds and of the X···N halogen bonds are also reported and compared with the experimental values. It is to be noted that the use of the Stuttgart/Dresden (SDD) effective core potential on the halogen atoms overestimates by more than 0.05 Å both the C−Br and C−I experimental bond lengths. On the other hand, all electron calculations allow to reproduce such intramolecular distances within the acceptable threshold of 0.02 Å.

By looking at the interaction energies obtained for the bromine complex before (ΔE_{uncorr}) and after ($\Delta E_{BSSEcorr}$) BSSE correction, it results that a suitable accuracy is get with the largest basis set used, 6-311++G**. However, the closeness of the $\Delta E_{BSSEcorr}$ values obtained at DFT level with this basis set and with the smaller MIDI! basis set makes us confident

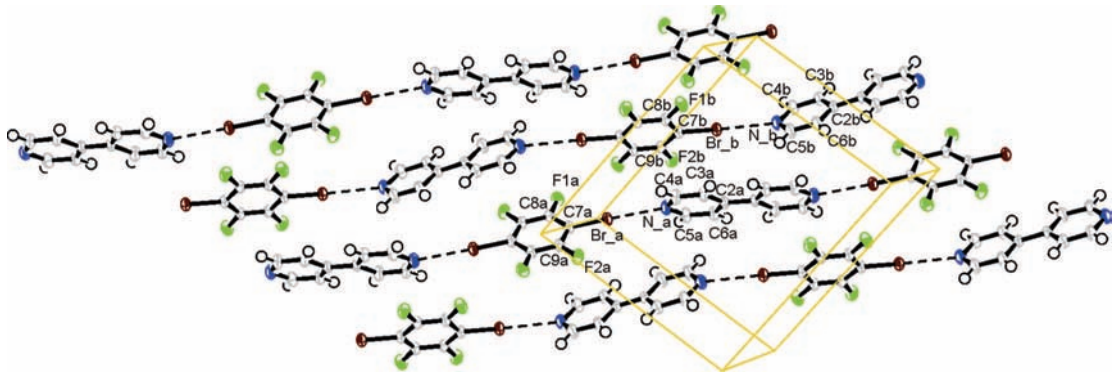

Figure 2. Packing diagram of dp·$C_6F_4Br_2$ at 90 K with atom numbering scheme. Ellipsoids at 90% probability level.

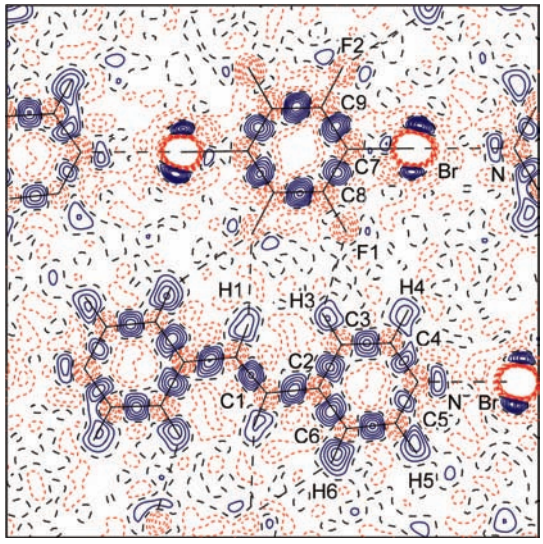

Figure 3. Deformation density map for bpe·$C_6F_4Br_2$ in the least-squares plane defined by the heavy atoms of $C_6F_4Br_2$ and $bpe_{1-x,-1-y,-1-z}$. The contour interval is 0.10 e Å^{-3}. Solid blue lines, positive contours; short dashed red lines, negative contours; wide dashed black lines, zero contours.

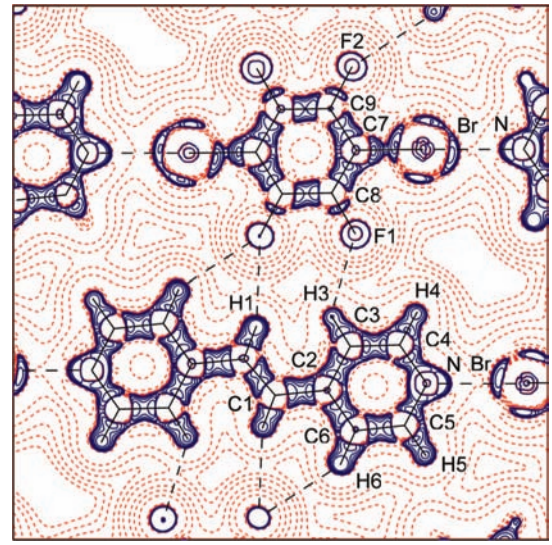

Figure 4. Laplacian, $\nabla^2\rho(\mathbf{r})$, of the experimental electron density of bpe·$C_6F_4Br_2$ in the least-squares plane defined by the heavy atoms of $C_6F_4Br_2$ and $bpe_{1-x,-1-y,-1-z}$. The absolute values of the contours (au) increase in steps of 2×10^n, 4×10^n, and 8×10^n with n beginning at -3 and increasing in steps of 1. Positive values are denoted by red dashed contours, negative values by blue solid contours.

about the reliability of the latter. Moreover, a very similar value of $\Delta E_{BSSEcorr}$ is obtained with the MP2/MIDI! wave function. These results allowed us to safely use the same MIDI! basis set for the iodine complex, for which both DFT and MP2 methods give interaction energies $\Delta E_{BSSEcorr}$ very close to each other.

Geometry optimizations on the potential energy surface corrected for BSSE have been performed for both complexes. The corresponding interaction energies ($\Delta E_{BSSEfree}$) well reproduce the $\Delta E_{BSSEcorr}$ values which were obtained without geometry relaxation. In the case of the bromine complex, this calculation does not imply a significant variation of the Br···N distance with respect to the value assumed in the unrelaxed calculation because, as said before, the 6-311++G** basis set is sufficiently extended to avoid BSSE. For the iodine complex, on the other hand, optimization on the BSSE free surface determines a lengthening of the I···N distance by 0.11, from DFT, or 0.17 Å, from MP2 calculations (see footnote [b] of Table 7), suggesting the existence of a fairly flat potential energy surface separating the halogen-bonded partners. This fact could explain their greater distance (by more than 0.1 Å) as computed for the gas-phase dimers with respect to that observed experimentally in the crystal.

Atomic Charges. Aimed at ascertaining a possible charge transfer character in the halogen bond interaction, we have determined the atomic charges by integration of electron density over the topological atomic basins Ω.[31] The molecular charges obtained for the investigated structures are reported in Table 8,[41] while the individual atomic contributions are given as Supporting Information. For bpe·$C_6F_4Br_2$, the sum over the atomic charges on the $C_6F_4Br_2$ module is +0.36(2) e, denoting a charge transfer from the halogenated molecule toward the Lewis base. The observed direction of charge transfer is then *opposite* to that found in the previously investigated iodine complexes bpe·$C_6F_4I_2$,[18] also reported in Table 8, and dpNO·$C_6F_4I_2$,[19] both of them having a charge equal to −0.40(2) e on the $C_6F_4I_2$ molecule.

For dp·$C_6F_4Br_2$, whose unit cell comprises two independent halogen-bonded dimers, an excess of charge, equal to −0.88 e, has been obtained on dimer A.[42] The observed charge transfer from dimer B to dimer A can be attributed to both their different geometry and the different crystal packing around each dimer, and indicates the importance of the isotropic terms of the intermolecular interactions, such as exchange-repulsion and dispersion, in determining the fine details of the interatomic surfaces and then the atomic charges. However, taking into account that the main local interaction is due to halogen bonding, we can still bring our attention to the charge transfer *within* each dimer. For dimer A, we obtained a charge transfer of 0.48(2) e from the Lewis base to the halogenated molecule, that is, in the *same* direction as the iodine complexes, while for dimer

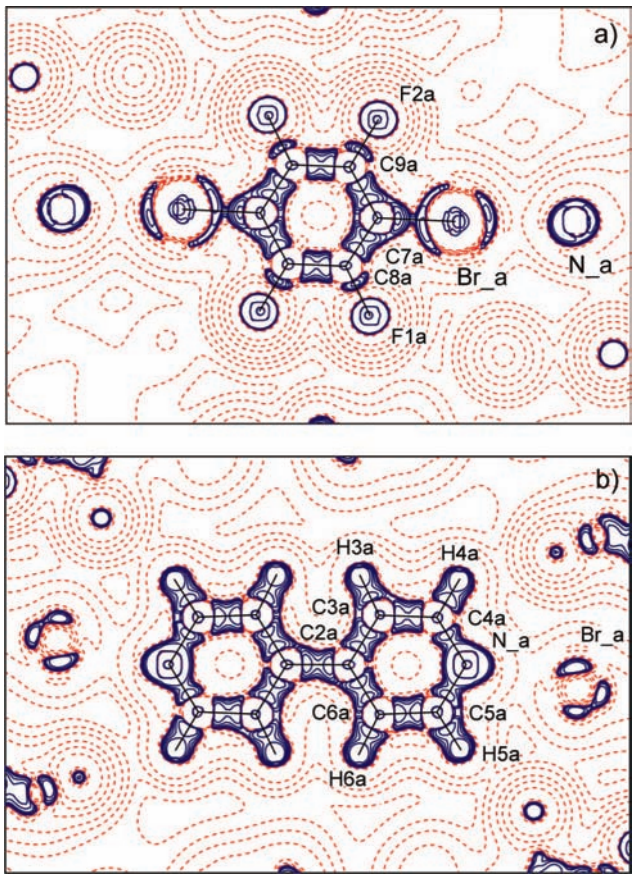

Figure 5. Laplacian, $\nabla^2\rho(\mathbf{r})$, of the experimental electron density of dp·$C_6F_4Br_2$ in the least-squares planes defined by the heavy atoms of (a) $C_6F_4Br_2$, molecule a; and (b) dp, molecule a. The absolute values of the contours (au) increase in steps of 2×10^n, 4×10^n, and 8×10^n with n beginning at -3 and increasing in steps of 1. Positive values are denoted by red dashed contours, negative values by blue solid contours.

TABLE 8: X-ray Derived (First Row) and Theoretical (Second Row)[a] Integrated Net Charges q (e) of the Halogen-Bonded Molecular Modules As Obtained by the QTAIM Partitioning[b]

		dp·$C_6F_4Br_2$		
	bpe·$C_6F_4Br_2$	dimer A	dimer B	bpe·$C_6F_4I_2$[c]
$\sum C_6F_4X_2$	0.36(2)	−0.68(2)	0.48(2)	−0.40(2)
	0.02	*0.00*		*−0.08*
$\sum$bpe/dp	−0.34(2)	−0.20(2)	0.56(2)	0.40(2)
	−0.02	*0.00*		*0.08*

[a] B3LYP/6-311++G** for bpe·$C_6F_4Br_2$ and dp·$C_6F_4Br_2$; B3LYP/MIDI! for bpe·$C_6F_4I_2$. [b] See Supporting Information for the individual atomic contributions. [c] Experimental values from ref 18, theoretical values from present work.

B the charge transfer was virtually zero within the integration error.[43] In conclusion, while for the iodine complexes the presence and the direction of charge transfer have been experimentally confirmed in two systems, and agree with what expected from the halogen-bonding definition,[1,2] for the bromine complexes neither the presence nor the direction of charge transfer, if any, seems to be reproducible. This is probably associated with the lower strength of the Br···N interaction with respect to the I···N or I···O halogen bonds.

The results of theoretical calculations are also reported in Table 8. Essentially no charge transfer is predicted for either of the bromine complexes, while a very small charge transfer, 0.08 e, is obtained for the iodine complex in the same direction as the experimental one, that is, from the Lewis base toward the halogenated molecule. By looking at the individual atomic contributions (see Supporting Information), the most striking discrepancy between theoretical and experimental results concerns the halogen atoms, whose net charges are always positive from theory and always negative or virtually zero from experiment. For almost all the other atoms, the sign of the net charges is reproduced, though calculations generally appear to overestimate the charges with respect to the values derived from experiment (see in particular the nitrogen atom).

4. Conclusions

The results of an electron density distribution study on the halogen-bonded bpe·$C_6F_4Br_2$ and dp·$C_6F_4Br_2$ complexes have been reported and compared with those previously obtained for the bpe·$C_6F_4I_2$ complex. The different nature of the Br and I halogen atoms has been elucidated through topological analysis of the electron density. The bromine atom shows four evident maxima in the valence shell charge concentration region, associated with its lone pairs, while the iodine atom is essentially characterized by a depletion of charge density in the valence region, though four maxima in the VSCC can be detected for this atom as well. This different charge distribution around the two halogen atoms determines a greater covalence degree for the C−Br than for the C−I bond. The former is in fact intermediate between *transit* closed shell and *pure* shared shell interaction, while the latter can be described as *transit* closed shell interaction.

A comparison between topological descriptors of the Br···N and I···N halogen bonds reveals a character at the boundary between *pure* and *transit* closed shell interaction for the former and a partial shared-shell character for the latter. Moreover, the presence of charge concentration maxima around the halogen atoms, located far from the directions of the intra- and intermolecular interactions, explains the strong directionality of the halogen-bonding interaction. Accurate evaluation of the interaction energies associated to Br···N and I···N halogen bonds gives, respectively, 3.22 (at B3LYP/6-311++G** level) and 5.37 kcal/mol (at B3LYP/MIDI! level).

The determination of the atomic charges from integration over the atomic basins shows that the charge transfer contribution to the halogen-bonding energy is not particularly significant for the examined complexes, confirming the predominantly electrostatic character of this interaction.[4,10−12]

Acknowledgment. The author thanks Dr. Riccardo Bianchi for helpful discussions and Professor Giuseppe Resnati for the supply of crystals. This work was partially supported by Fondazione Cariplo (Project Self-Assembled Nanostructured Materials: A Strategy for the Control of Electrooptic Properties).

Supporting Information Available: Final atomic fractional coordinates; anisotropic, isotropic and cumulant thermal parameters; multipole population; residual and deformation density maps. This material is available free of charge via the Internet at http://pubs.acs.org.

References and Notes

(1) Metrangolo, P., Resnati, G., Eds.; *Halogen Bonding: Fundamentals and Applications*; Springer: Berlin, 2008, and references therein.

(2) (a) Desiraju, G. R.; Harlow, R. L. *J. Am. Chem. Soc.* **1989**, *111*, 6757–6764. (b) Bailey, R. D.; Grabarczyk, M.; Hanks, T. W.; Pennington, W. T. *J. Chem. Soc., Perkin Trans.* **1997**, *2*, 2781–2786. (c) Metrangolo, P.; Neukirch, H.; Pilati, T.; Resnati, G. *Acc. Chem. Res.* **2005**, *38*, 386–

395. (d) Metrangolo, P.; Meyer, F.; Pilati, T.; Resnati, G.; Terraneo, G. *Angew. Chem., Int. Ed.* **2008**, *47*, 6114–6127.

(3) (a) Fourmigué, M.; Batail, P. *Chem. Rev.* **2004**, *104*, 5379–5418. (b) Shirahata, T.; Kibune, M.; Maesato, M.; Kawashima, T.; Saito, G.; Imakubo, T. *J. Mater. Chem.* **2006**, *16*, 3381–3390. (c) Metrangolo, P.; Präsang, C.; Resnati, G.; Liantonio, R.; Whitwood, A. C.; Bruce, D. W. *Chem. Commun.* **2006**, 3290–3292. (d) Xu, J.; Liu, X.; Kok-Peng Ng, J.; Lin, T.; He, C. *J. Mater. Chem.* **2006**, *16*, 3540–3545. (e) Sarma, J. A. R. P.; Allen, F. H.; Hoy, V. J.; Howard, J. A. K.; Thaimattam, R.; Biradha, K.; Desiraju, G. R. *Chem. Commun.* **1997**, 101–102. (f) Thallapally, P. K.; Desiraju, G. R.; Bagieu-Beucher, M.; Masse, R.; Bourgogne, C.; Nicoud, J. F. *Chem. Commun.* **2002**, 1052–1053. (g) Cariati, E.; Forni, A.; Biella, S.; Metrangolo, P.; Meyer, F.; Resnati, G.; Righetto, S.; Tordin, E.; Ugo, R. *Chem. Commun.* **2007**, 2590–2592. (h) Kamal Boubekeur, K.; Syssa-Magalé, J.-L.; Palvadeau, P.; Schöllhorn, B. *Tetrahedron Lett.* **2006**, *47*, 1249–1252.

(4) Auffinger, P.; Hays, F. A.; Westhof, E.; Ho, P. S. *Proc. Natl. Acad. Sci. U.S.A.* **2004**, *101*, 16789–16794.

(5) Wojtczak, A.; Cody, V.; Luft, J. R.; Pangborn, W. *Acta Crystallogr., Sect. D* **2001**, *57*, 1061–1070.

(6) (a) Howard, E. I.; Sanishvili, R.; Cachau, R. E.; Mitschler, A.; Chevrier, B.; Barth, P.; Lamour, V.; Van Zandt, M.; Sibley, E.; Bon, C.; Moras, D.; Schneider, T. R.; Joachimiak, A.; Podjarny, A. *Proteins* **2004**, *55*, 792–804. (b) Muzet, N.; Guillot, B.; Jelsch, C.; Howard, E.; Lecomte, C. *Proc. Natl. Acad. Sci. U.S.A.* **2003**, *100*, 8742–8747.

(7) (a) Hassel, O.; Hvoslef, J. *Acta Chem. Scand.* **1954**, *8*, 1953. (b) Hassel, O. *Mol. Phys.* **1958**, 241–246. (c) Hassel, O. *Science* **1970**, *170*, 497–502. (d) Bent, H. A. *Chem. Rev.* **1968**, *68*, 587–648.

(8) Metrangolo, P.; Resnati, G. *Chem. Eur. J.* **2001**, *7*, 2511–2519.

(9) (a) De Santis, A.; Forni, A.; Liantonio, R.; Metrangolo, P.; Pilati, T.; Resnati, G. *Chem. Eur. J.* **2003**, *9*, 3974–3983. (b) Forni, A.; Metrangolo, P.; Pilati, T.; Resnati, G. *Cryst. Growth Des.* **2004**, *4*, 291–295. (c) Walsh, R. B.; Padgett, C. W.; Metrangolo, P.; Resnati, G.; Hanks, T. W.; Pennington, W. T. *Cryst. Growth Des.* **2001**, *1*, 165–175. (d) Corradi, E.; Meille, S. V.; Messina, M. T.; Metrangolo, P.; Resnati, G. *Angew. Chem., Int. Ed.* **2000**, *39*, 1782–1786.

(10) Lommerse, J. P. M.; Stone, A. J.; Taylor, R.; Allen, F. H. *J. Am. Chem. Soc.* **1996**, *118*, 3108–3116.

(11) (a) Brinck, T.; Murray, J. S.; Politzer, P. *Int. J. Quantum Chem. Quantum Biol. Symp.* **1992**, *44*, 57–64. (b) Politzer, P.; Lane, P.; Concha, M. C.; Ma, Y.; Murray, J. S. *J. Mol. Model.* **2007**, *13*, 305–311.

(12) (a) Clark, T.; Hennemann, H.; Murray, J. S.; Politzer, P. *J. Mol. Model.* **2007**, *13*, 291–296. (b) Politzer, P.; Murray, J. S.; Lane, P. *Int. J. Quantum Chem.* **2007**, *107*, 3046–3052. (c) Murray, J. S.; Concha, M. C.; Lane, P.; Hobza, P.; Politzer, P. *J. Mol. Model.* **2008**, *14*, 699–704.

(13) Wang, W. Z.; Wong, N. B.; Zheng, W. X.; Tian, A. M. *J. Phys. Chem. A* **2004**, *108*, 1799–1805.

(14) Zou, J. W.; Jiang, Y. J.; Guo, M.; Hu, G. X.; Zhang, B.; Liu, H. C.; Yu, Q. S. *Chem. Eur. J.* **2005**, *11*, 740–751.

(15) Wang, W.; Hobza, P. *J. Phys. Chem. A* **2008**, *112*, 4114–4119.

(16) Hermansson, K. *J. Phys. Chem. A* **2002**, *106*, 4695–4702.

(17) Qian, W.; Krimm, S. *J. Phys. Chem. A* **2002**, *106*, 6628–6636.

(18) Bianchi, R.; Forni, A.; Pilati, T. *Chem. Eur. J.* **2003**, *9*, 1631–1638.

(19) Bianchi, R.; Forni, A.; Pilati, T. *Acta Crystallogr. Sect. B* **2004**, *60*, 559–568.

(20) Stewart, R. *Acta Crystallogr., Sect. A* **1976**, *32*, 565–574.

(21) Bianchi, R.; Forni, A. *J. Appl. Crystallogr.* **2005**, *38*, 232–236.

(22) Clementi, E.; Roetti, C. *At. Data Nucl. Data Tables* **1974**, *14*, 177–478.

(23) (a) Hehre, W. J.; Ditchfield, R.; Stewart, R. F.; Pople, J. A. *J. Chem. Phys.* **1970**, *52*, 2769–2773. (b) Pietro, W. J.; Levi, B. A.; Hehre, W. J.; Stewart, R. F. *Inorg. Chem.* **1980**, *19*, 2225–2229.

(24) Frisch, M. J.; Trucks, G. W.; Schlegel, H. B.; Scuseria, G. E.; Robb, M. A.; Cheeseman, J. R.; Montgomery Jr., J. A.; Vreven, T.; Kudin, K. N.; Burant, J. C.; Millam, J. M.; Iyengar, S. S.; Tomasi, J.; Barone, V.; Mennucci, B.; Cossi, M.; Scalmani, G.; Rega, N.; Petersson, G. A.; Nakatsuji, H.; Hada, M.; Ehara, M.; Toyota, K.; Fukuda, R.; Hasegawa, J.; Ishida, M.; Nakajima, T.; Honda, Y.; Kitao, O.; Nakai, H.; Klene, M.; Li, X.; Knox, J. E.; Hratchian, H. P.; Cross, J. B.; Bakken, V.; Adamo, C.; Jaramillo, J.; Gomperts, R.; Stratmann, R. E.; Yazyev, O.; Austin, A. J.; Cammi, R.; Pomelli, C.; Ochterski, J. W.; Ayala, P. Y.; Morokuma, K.; Voth, G. A.; Salvador, P.; Dannenberg, J. J.; Zakrzewski, V. G.; Dapprich, S.; Daniels, A. D.; Strain, M. C.; Farkas, O.; Malick, D. K.; Rabuck, A. D.; Raghavachari, K.; Foresman, J. B.; Ortiz, J. V.; Cui, Q.,; Baboul, A. G.; Clifford, S.; Cioslowski, J.; Stefanov, B. B.; Liu, G.; Liashenko, A.; Piskorz, P.; Komaromi, I.; Martin, R. L.; Fox, D. J.; Keith, T.; Al-Laham, M. A.; Peng, C. Y.; Nanayakkara, A.; Challacombe, M.; Gill, P. M. W.; Johnson, B.; Chen, W.; Wong, M. W.; Gonzalez, C.; Pople, J. A. *Gaussian 03, Revision D.01*; Gaussian Inc.: Pittsburgh, PA, 2003.

(25) Lee, C.; Yang, W.; Parr, R. G. *Phys. Rev. B* **1988**, *37*, 785–789.

(26) Becke, A. D. *J. Chem. Phys.* **1993**, *98*, 5648–5652.

(27) Boys, S. F.; Bernardi, F. *Mol. Phys.* **1970**, *19*, 553–566.

(28) Bader, R. F. W. *AIMPAC: A set of programs for the theory of atoms in molecules*; McMaster University: Hamilton, Ontario, Canada L8S 4M1, 1994.

(29) Saunders, V. R.; Dovesi, R.; Roetti, C.; Causà M., Harrison, N. M.; Orlando, R.; Zicovich-Wilson, C. M. *CRYSTAL98 User'S Manual*; University of Torino, Torino, Italy, 1998.

(30) Gatti, C. *TOPOND-98: an electron density topological program for systems periodic in N (N = 0−3) dimensions, User's Manual*; CNR-CSRSRC, Milan, Italy;http://www.istm.cnr.it/∼gatti/TOPOND.ppt, 1999.

(31) Bader, R. F. W. *Atoms in Molecules-A Quantum Theory*; Oxford University Press: Oxford, UK, 1994.

(32) Bondi, A. *J. Phys. Chem.* **1964**, *68*, 441–451.

(33) Note that the different appearance of the contour levels around bromine in parts a and b of Figure 5 is due to the noncoplanarity of the two molecular modules. The two parts are in fact plotted in different molecular planes.

(34) Bader, R. F. W.; Beddall, P. M. *J. Chem. Phys.* **1972**, *56*, 3320–3329.

(35) Abramov, Yu. A. *Acta Crystallogr., Sect. A* **1997**, *53*, 264–272.

(36) Espinosa, E.; Molins, E.; Lecomte, C. *Chem. Phys. Lett.* **1998**, *285*, 170–173.

(37) Espinosa, E.; Alkorta, I.; Elguero, J.; Molins, E. *J. Chem. Phys.* **2002**, *117*, 5529–5542.

(38) Koritsanszky, T. S.; Coppens, P. *Chem. Rev.* **2001**, *101*, 1583–1627.

(39) Matta, C. F.; Hernández-Trujillo, J.; Tang, T.-H.; Bader, R. F. W. *Chem. Eur. J.* **2003**, *9*, 1940–1951.

(40) Hibbs, D. E.; Overgaard, J.; Platts, J. A.; Waller, M. P.; Hursthouse, M. B. *J. Phys. Chem. B* **2004**, *108*, 3663–3672.

(41) The values of molecular charge reported here and in Table 8 refer in all cases to full molecules, but integration of course has been done on only the independent half molecule.

(42) Note that there is not an equal and opposite charge on dimer B, which in fact lacks 1.04(2) e (0.52(2) e on the asymmetric unit), owing to the error connected to the integration procedure (see section 2 (Methods: Evaluation of Atomic Charges).

(43) The occurrence of charge transfer from one independent dimer of $dp \cdot C_6F_4Br_2$ to the other one prompted us to perform further multipole refinements of this structure where the core and the spherical valence populations of each atom of a dimer were constrained to be equal to those of the corresponding atoms of the other dimer of the asymmetric unit. This refinement did not imply any significant variation in the topological properties at BCPs and, obviously, no charge transfer between dimers has been obtained. In this case, charge transfer within each dimer was virtually zero.

JP8107182